Wake Structure Induced by Seal Whisker: Effects of Angle of Incidence

Aidan W. Rinehart* Wei Zhang†

Cleveland State University, 2121 Euclid Ave, Cleveland, OH 44115.

Vikram Shyam‡

NASA Glenn Research Center, 21000 Brookpark Road Cleveland, OH 44135

Seal whiskers have been found to produce unique wake flow structures that minimize self-induced vibration and reduce drag. The cause of these wake features are due to the peculiar three-dimensional morphology of the whisker surface. The whisker can be defined as an elliptical cross section with variation in the major and minor axis of the ellipse along the length of the whisker as well as rotation of the elliptical plane with respect to the whisker axis, angle of incidence. While the effects of several dominant parameters of the whisker morphology have been studied, the effect of the rotation of the elliptical plane has not been well understood. This paper will examine the influence of the angle of incidence on the wake flow structure through series of water channel studies. Several models of whisker-like geometries will be tested which isolate the rotation angle as the only variation between models. The wake structure behind each seal whisker model will be measured through particle image velocimetry (PIV). The different models' wake structures will be compared identifying the effect of angle of incidence on the wake structure. Angle of incidence was found to influence the wake structure through reorganization of velocity patterns, reduction of recovery length and modification of magnitude of T_u. These results help provide a more complete understanding of the seal whisker geometry relationship to wake structure and can provide insight into design practices for application of whisker geometery to various engineering problems.

Nomenclature

α	Ange of incidence at the peak location
a	Diameter of major axis at peak location
β	Angle of incidence at the trough location
b	Diameter of minor axis at peak location
D_m	Average diameter of four elliptical diameters
k	Diameter of major axis at trough location
l	Diameter of minor axis at trough location
M	Distance between peak and trough location
Re	Reynolds Number
u	Velocity in the x direction
U_o	Freestream Velocity
T_u	Turbulence intensity of the u velocity component

*Graduate Student, Mechanical Engineering, 2121 Euclid Ave, Cleveland, OH 44115, AIAA Student Member.

† Assistant Professor, Mechanical Engineering, 2121 Euclid Ave, Cleveland, OH 44115, AIAA Member.

‡ Propulsion Flow Dynamicist, Turbo Machinery and Heat Transfer, 21000 Brookpark Road Cleveland, OH 44135, AIAA Member

I. Introduction

There exist certain species of seals that possess whiskers featuring undulating surfaces. These types of whiskers have recently become an area of interest due to the unique flow features they produce. The Harbor seal whisker was hypothesized to aid in the tracking of prey.[1,8] Research revealed that the unique undulating surface of the Harbor seal produced a flow behind the whisker that changes the von Karman vortex street and ultimately reduces the whisker vibrations. This reduction in vibration allows the seal to sense smaller fluctuations within the incoming flow, such as the wake of a fish and in turn enhance the seal's ability to track the fish. Others have contributed to the surface geometry characterization of different seal species capturing standard morphology parameters; wavelength, width and length measurements.[2, 3, 5, 11] Another study investigated the vibration effects of the whisker's angle of orientation to the flow.[4] Yet another study dissected the different features of undulating whisker geometry and related those to the forces acting on the whisker.[6] Their method looked at five different whisker-like geometries attempting to understand how each type of morphology feature affects the trailing flow. Additionally research has been presented applying the similar geometry of the undulating whisker surface to flow sensor design as well as turbine blade design.[9,10] It has been hypothesized that the major axis angle is significantly smaller than that reported previously and may not play as significant a role in wake modification at high Reynolds number.[11] Regarding characterization of the seal whisker morphology, a comparison of various methods was conducted. It was determined that CT scans were the most reliable and useful to both capture morphology and to create scaled-up 3D models for wind tunnel testing.[12] This brief overview shows much effort has been applied to understanding the features and effects of undulating whiskers? morphology on adjacent wake structure. However, there are a number of remaining questions and uncertainties within this field. In particular, one question that has not been well resolved is the effect of the angle of incidence that produces an offset between the leading edge and trailing edge peaks and troughs. Most studies have applied a constant angle of incidence to the whole model while a few have noticed the existence, but have not resolved the role this feature plays. The objective of this paper is to obtain more comprehensive understanding of the role the rotation angle plays in the wake structure through series of water channel tunnel testing.

II. Theory

Much of the interest in understanding and studying the seal whiskers can be traced back to the von Karman Vortex Street phenomena. Blunt objects in flow experience von Karman Vortex Street at a sufficiently high Reynolds number. This is the phenomena where large vortices are shed in a periodic fashion in the wake of the blunt object as depicted in Fig. 1.

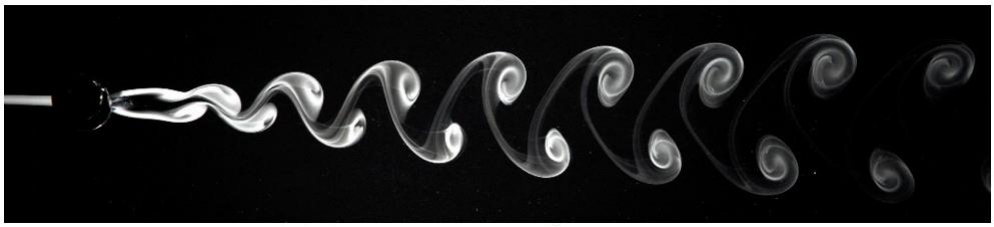

Figure 1: von Karman Vortex Street Behind a Circular Cylinder[13]

The seal whisker, due to its geometry, suppresses the formation of these vortices. The Harbor seal is one seal species that displays the complex undulating geometry and was the whisker modeled in the Hanke 2010 paper.[1] An example of a Harbor seal whisker is provided below in Fig. 2 to illustrate the unique geometry found in nature.

This geometry is very complex, a method for characterized the whisker geometry was suggested by Hanke et al. and will be used in this research as well.[1] The characterization is accomplished using a seven parameter definition depicted below in Fig. 3.

Ellipse definitions are measured at the locations where the x-axis width is at a maximum, henceforth referred to as peak, and when the width is a minimum, henceforth referred to as trough. The parameters definitions are as follows; a defines the major axis of the ellipse defined at the peak, b defines the minor axis of the ellipse at the peak, k is the major axis of the ellipse at the trough and l is the minor axis of the ellipse

Figure 2: Magnified Harbor Seal Whisker

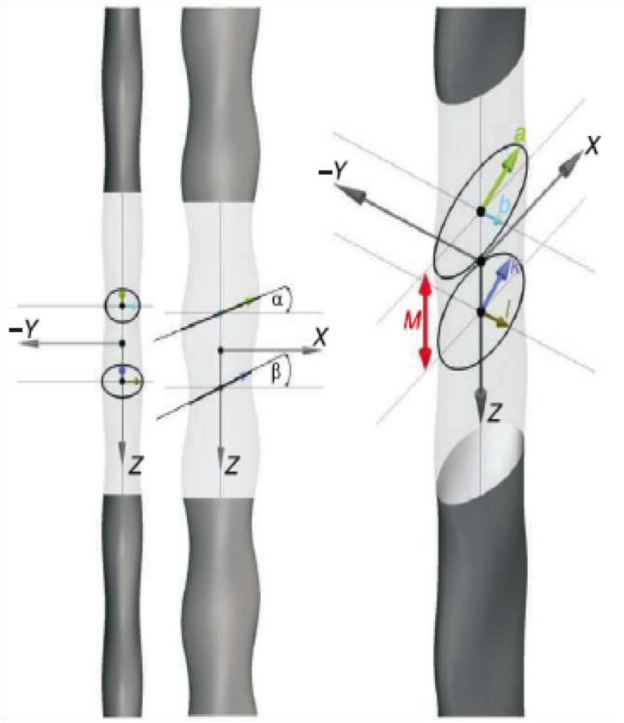

Figure 3: 7 Parameter Whisker Definition provided by Hanke et. al[1]

at the trough. M defines the wavelength or distance between the peak and trough. Finally the elliptical plane rotation angles are defined by α at the peak location and β at the trough location.

Previous studies to this point have simplified the complex three-dimensional geometry to provide an easier problem to study. One simplification made is the assumption of a constant angle for the elliptical plane rotation. While this assumption does simplify the geometry of the whisker it may not provide an accurate representation of the wake structure. Literature is sparse to non-existent when it comes to characterizing the angle which defines the elliptical plane rotation of the seal whisker. In our previous work, 27 seal whiskers were analyzed with a North Star Imaging Company CT scanner located at the NASA Glenn Research Center.[12] This analysis provided measurements that fully defined the whisker per the seven parameter nomenclature used by Hanke et al. The prior study addressed the knowledge gap pertaining to the angle of incidence. That study found the seal whisker angle of incidence exhibit a wide variation from whisker to whisker as well as along the length of each whisker. A brief summary of the results are provided in the figure below for further details the reader is referred to work conducted by Rinehart et. al.[12] Figure 4 shows the frequency of different ranges of angles of incidence that were measured within previous studies.

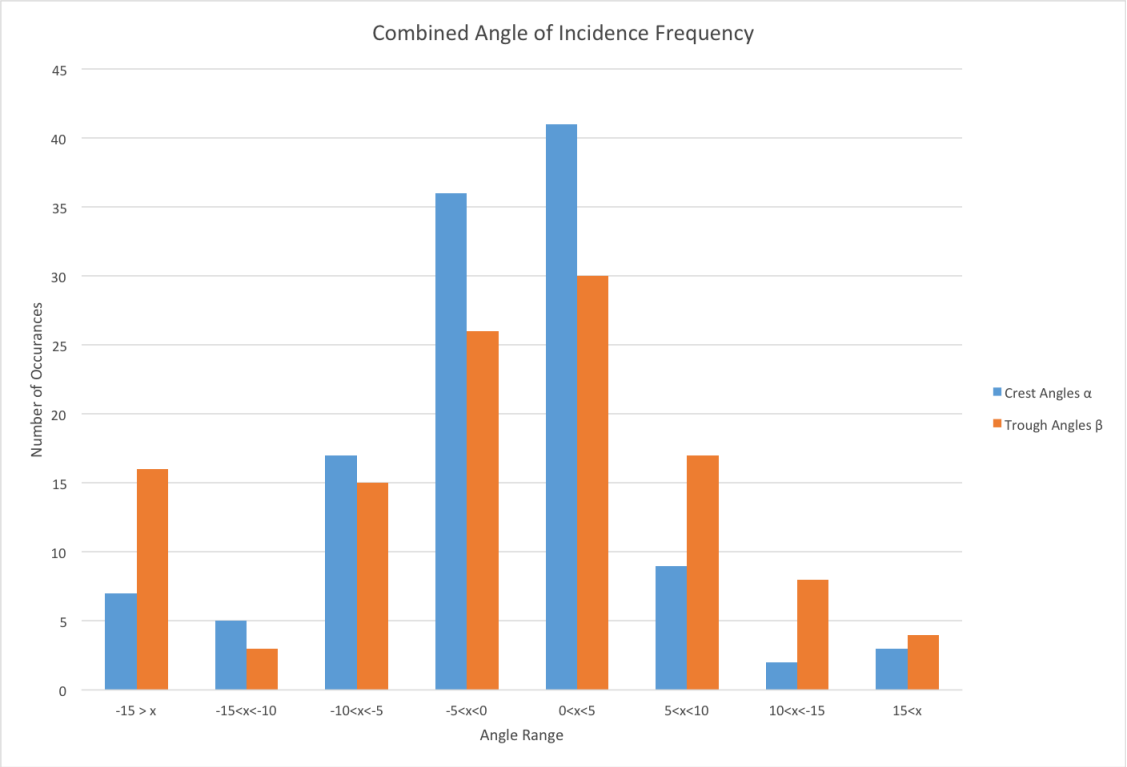

Figure 4: Angle of Incidence Frequency of Occurrence

Figure 4 shows a clustering of distribution of angles around 0° with only a few instances having rotations greater than 0°. It naturally leads to the following questions; what effect does the angle of rotation have on the wake structure and is there a way to improve on the observed natural design. The remainder of this research will be focused on addressing these questions.

III. Experimental Setup

III.A. Whisker Model

The influence the angle of incidence has on the wake structure is not well understood. To address this knowledge gap an in depth study of the whisker geometry found in nature was conducted in the previous chapter. The results of morphology study supplied the parameters to define and construct representative whisker models. The following flow study will focus on the Harbor seal geometry. The mean values found in the morphology study were used to define the values for major and minor axis at the peak location, a and b, the major and minor axis at the trough location, k and l, and the distance between the peak and

trough M. For comparison and nondimensionalization purposes it is helpful to have a single value describing the cross section of the model, D_m, for this study an average of the four diameters that define the peak and trough ellipses will be used. These values were then scaled up roughly eight times the size of real Harbor seal whiskers to provide a sufficient number of undulations within the water channel test section while remaining within the resolution of the 3D printer. From here three models were constructed; model A with 0° angle of incidence for both α and β, model B with 15° angle of incidence for both α and β, and model C with 5° angle of incidence for α and 5° angle of incidence for β. These models were generated using the Solid Works tool. Elliptical cross-sections were created on planes that provided the proper angle of incidence to the axis of the model and were spaced to maintain the correct half wavelength defining the distance between the peak and trough locations observed in the whisker morphology study. The loft feature was applied to the different cross-sections to create the three dimensional whisker models. The dimensions of the common geometry are provided in the table **1**.

Table 1: Whisker Model Geometry

	a (mm)	b (mm)	l (mm)	k (mm)	M (mm)	λ/Dm	# undulation
Whisker Model Parameters	7.73	2.62	6.20	2.92	12.70	5.22	4.5

III.B. Water Channel

A water channel provided the flow environment used to study the wake structure created by the seal whisker models. The water channel is constructed with plexiglass sheets. The water channel consists of a stacked flow path were water is pumped into the upper channel containing the test section and returns to the reservoir by a return path immediately underneath the test section flowing in the opposite direction. The test section for the water channel consisted of a 0.14 m × 0.20 m × 0.61 m volume. The water channel used a constant speed pump that generated a flow with $R_e = 630$ where the length parameter is D_m. The flow was conditioned by six honeycomb flow straightener sections upstream of the test section. The water channel is characterized by a turbulence intensity of 4 %. An image of the experimental setup is provided in figure 5.

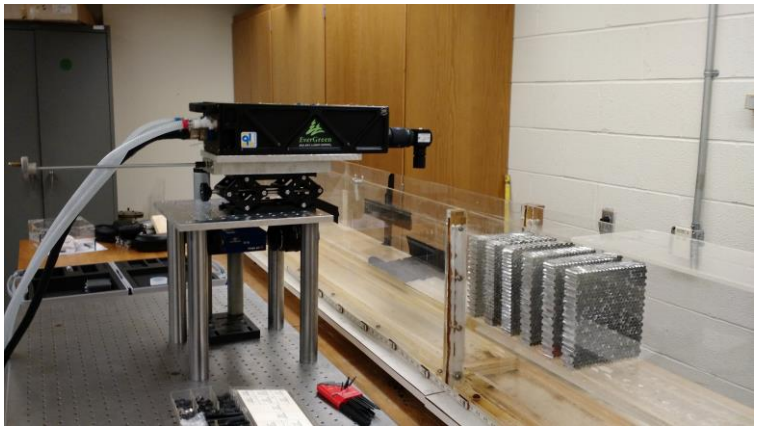

Figure 5: CSU Water Channel PIV Setup

Figure 5 shows the water channel with the 6 honeycomb flow conditioning devices upstream of the test section. The laser and camera are mounted on the adjustable platform. The laser is mounted on the top section of the platform with optic extending over the water channel and positioning the laser to direct the light sheet down the center line of the water channel. The camera is mounted below the laser between the platform legs.

The 3D printed whisker models were mounted in the center of the water channel test section and aligned to have zero angle of attack with respect to the incoming flow.

III.C. Particle Image Velocimetry

Characterization of the wake structure was accomplished through particle image velocimetry (PIV). PIV is a non-intrusive measurement technique for measuring flow conditions. The task is performed by seeding the flow being studied with particles of consistent size. These particles are then illuminated with laser light that has been constructed at a specific wavelength. The laser is then pulsed twice in a short amount of time. A camera that is fitted with a wavelength bandwidth filter specified to only capture the light from the laser captures two images timed with the laser pulses. The distance traveled by each particle illuminated by the laser light from the first image to the second image is calculated and with the known time step between laser pulses velocities can be obtained. There are numerous variations to PIV setups the one used in this research is a simple two dimensional two component setup. This means that a single camera captures a two dimensional image and from those two dimensional images two velocity components can be resolved. Images were captured for three setups for each whisker model. A vertical plane along the centerline of the whisker, a cross-sectional plane located at the peak of the whisker model and a cross-sectional plane located at the trough of the whisker model. A schematic of the measurement planes with respect to a representative whisker model is provided in figure 6 as well as the axis and velocity component definitions.

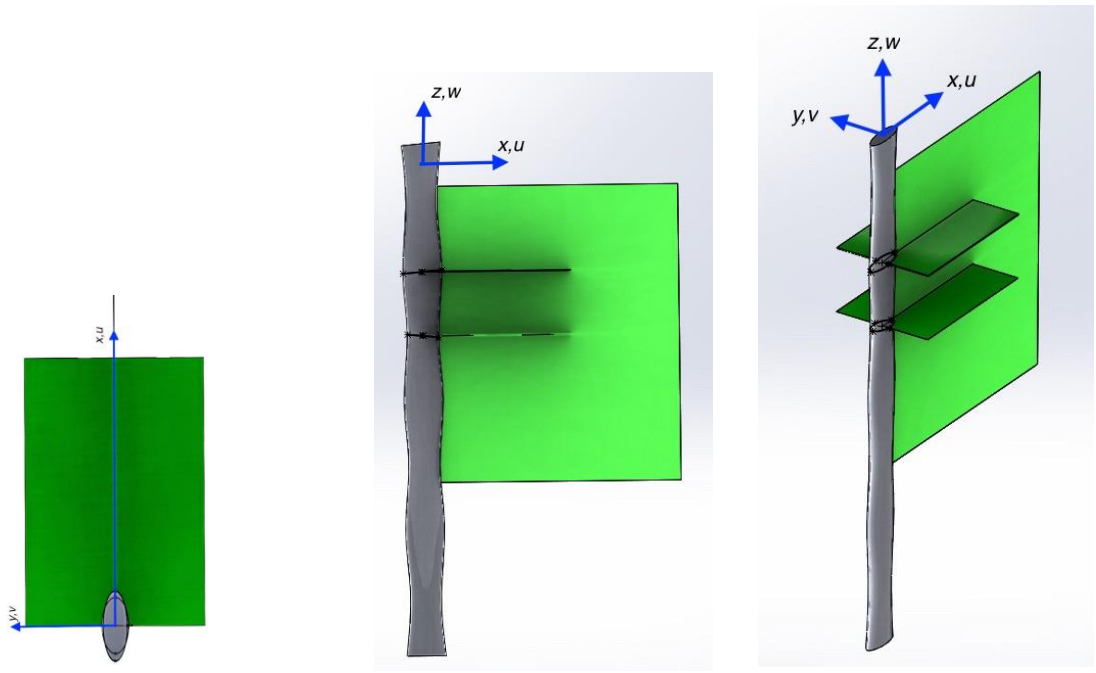

(a) Horizontal Measurement Plane (b) Vertical Measurement Plane (c) Vertical Measurement Plane

Figure 6: Measurement Plane Schematic

IV. Wake Structure Downstream of Seal Whisker

Three different whisker models will be examined in the following section. Each model tested in the water channel had 2000 image pairs taken in each of the three measurement planes to characterize the wake structure. These image pairs were processed to calculate velocity vectors depicting the fluid dynamics of the wake. The 2000 image pairs were then ensemble averaged to provide mean velocity fields as well as turbulence statistics. The following results show the characterization of the u velocity field as well as the T_u field in the three measurement planes. The x,y,z axis have been normalized with the parameter D_m, an average of the four diameters defining the ellipse cross section at the peak and trough locations.

IV.A. Mean u/U_o Velocity Fields

This section will focus on the u velocity fields for all three measurement planes. Figure 7 contains the mean u velocity normalized with the free stream velocity along the vertical centerline of the whisker models. The flow enters from the left side of the image and flows to the right side of the image. Half of the whisker model is shown in black on the far left side of the image providing the location of the peak and trough positions. The black lines extending from the model are extensions of the angle of incidence, α and β, to indicate position of wake structure in reference to the angle of incidence downstream of the model.

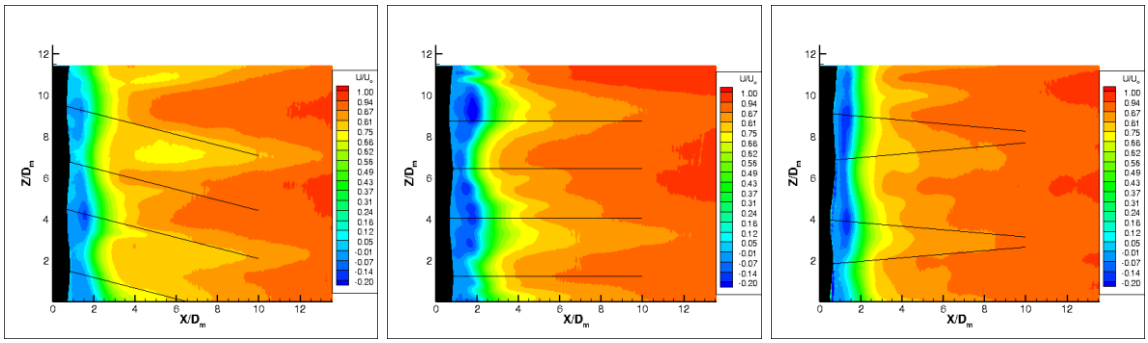

(a) Model C ($\alpha = -15^\circ$ $\beta = -15^\circ$) (b) Model A ($\alpha = 0^\circ$ $\beta = 0^\circ$) (c) Model B ($\alpha = 5^\circ$ $\beta = -5^\circ$)

Figure 7: Mean u/U_o Velocity Fields

The u velocity field behind the model A is characterized by a reversed flow region immediately following the whisker model. The flow then begins to recover and shows mirroring of the whisker geometry. The flow recovers in the shortest distance downstream inline with the peak geometries. The trough geometry recovers the slowest. The region inline with the troughs tend to recover at nearly twice the distance downstream as the regions inline with the peaks.

The u velocity field behind model B has a region of reverse flow right behind the whisker model. The largest regions of reverse flow are inline with the trough locations and the most narrow occur behind the peak locations. The flow begins to recover between one and two D_m downstream of the whisker model. The flow recovers to the free stream velocity consistently across the length of the model near 6 D_m.

The u velocity field behind model C has a reversed flow region immediately following the whisker model followed by a recovery of u velocity. The regions behind the peaks show slightly shorter recovery distances in the near wake, less than 4 D_m, where the regions behind the trough locations show longer distances required for the same amount of velocity recovery. Beyond 4 D_m the differences between peak and trough locations becomes much less distinct.

Figure 8 displays the mean u flow normalized with the free stream velocity. This data set is observing the flow looking down at the model with half of the peak elliptical cross section of the model visible on the left side of the figure. The flow is entering from the left and flowing towards the left of the figure.

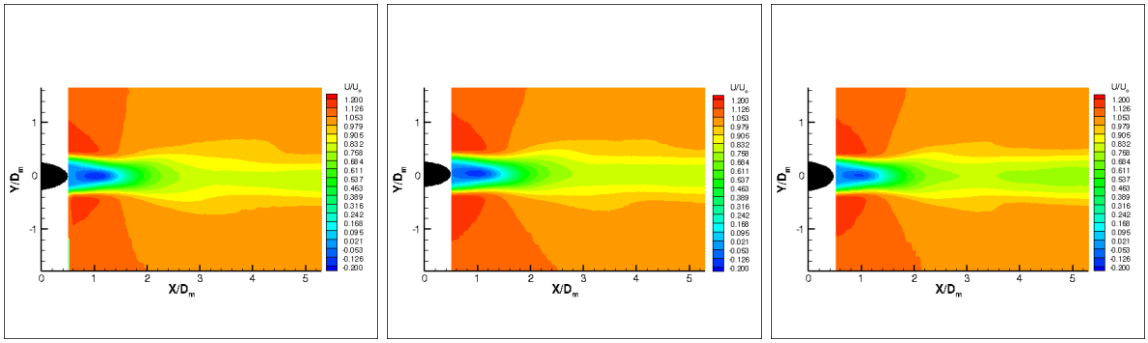

(a) Model C ($\alpha = -15^\circ$ $\beta = -15^\circ$) (b) Model A ($\alpha = 0^\circ$ $\beta = 0^\circ$) (c) Model B ($\alpha = 5^\circ$ $\beta = -5^\circ$)

Figure 8: Peak Mean u/U_o Velocity Fields

Model A has a region of reverse flow that extends to 1.5 X/D_m and then begins to recover. The flow

along the centerline of the model never fully recovers within this measurement window. The wake shows a slight growth in width that occurs just beyond the reverse flow region and then stabilizes at 0.5 D_m on either side of the whisker model.

Model B has a reversed flow region that extends 1.2 X/Dm downstream. The flow begins to recover until 3.6 X/D_m downstream where the flow experiences a reduction in u at the centerline. The reduced u is restricted to the center of the wake and reaches 0.25 D_m in both directions off the centerline. The wake velocity never fully recovers within this measurement window.

Model C has a reversed flow region extending to 1.5 X/D_m. The wake shows a slight expansion in the y-axis beginning at 1.5 X/D_m and reaching a maximum width of 0.5 D_m in either direction off the centerline. The u velocity begins recovering at 1.5 X/D_m until 4.2 X/D_m where u begins to reduce slightly. The flow in the wake does not fully recover within the measurement window.

Figure 9 contains the u flow normalized with the free stream velocity. Again the model is being viewed from above with half of the trough elliptical cross section visible on the left of the image. Flow enters the image from the left and flows to the right.

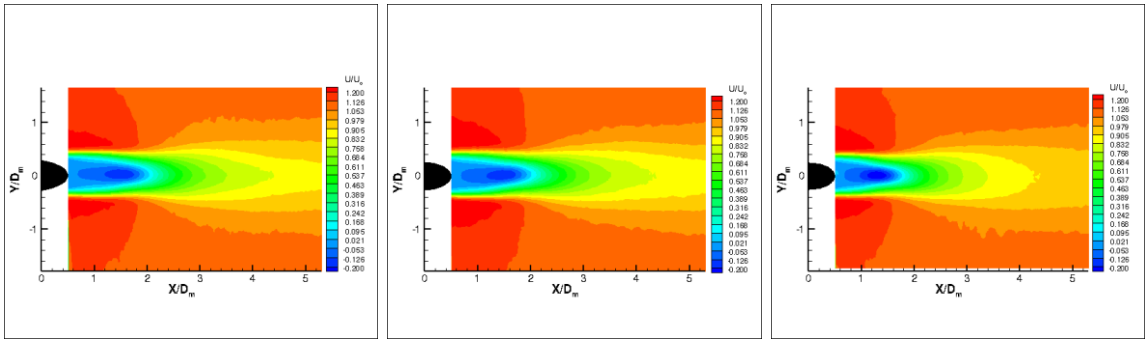

(a) Model C ($\alpha = -15^\circ$ $\beta = -15^\circ$) (b) Model A ($\alpha = 0^\circ$ $\beta = 0^\circ$) (c) Model B ($\alpha = 5^\circ$ $\beta = -5^\circ$)

Figure 9: Trough Mean u/U_o Velocity Fields

Model A has a reversed flow region that extends from the model to 2.0 X/D_m downstream. The u flow then begins to recover not fully reaching the free stream velocity condition within the measurement window. The flow recovers to 90% of the free stream flow at 4.2 X/D_m. The wake of reduced u velocity extends between 0.6 and -0.6 Y/D_m.

Model B has a reversed flow region that extends from the model to 1.7 X/D_m downstream. The u flow then begins to recover reaching 90% of the free stream flow at 3.4 X/D_m and then fully recovering near 4.2 X/D_m downstream. The wake of reduced u velocity extends between 0.6 and -0.6 Y/D_m.

Model C has a reversed flow region that extends from the model to 1.9 X/D_m downstream. The u flow then begins to recover reaching 90% of the free stream flow at 3.6 X/D_m and then fully recovering near 4.2 X/D_m downstream. The wake of reduced u velocity extends between 0.6 and -0.6 Y/D_m.

IV.B. Mean T_u Field

This section will focus on the turbulence intensity of the u velocity component. This parameter represents the amount of fluctuation present in the u velocity fields as a percentage of the free stream velocity defined by 1.

$$T_u = \frac{\sqrt{\overline{u^{t2}}}}{U_o} \tag{1}$$

Figure 10 displays the mean T_u field in percent units. The half of the model is represented in black on the left edge of the figure with angle of incidence lines extending from the model downstream.

Model A shows a region of very low T_u immediately following the whisker model. The low T_u is followed by a higher region of about 20% T_u with narrow segments of intensity between 27 and 30% T_u. The regions of 20% T_u extend parallel to the angle of incidence extension lines. These bands of 20% T_u are offset slightly from the mid points of the peak and trough locations. The regions directly inline with a peak or trough tend to have much lower T_u. The band of 20% T_u begin to see a reduction around 7 D_m downstream and have undergone significant reduction by 10 D_m downstream.

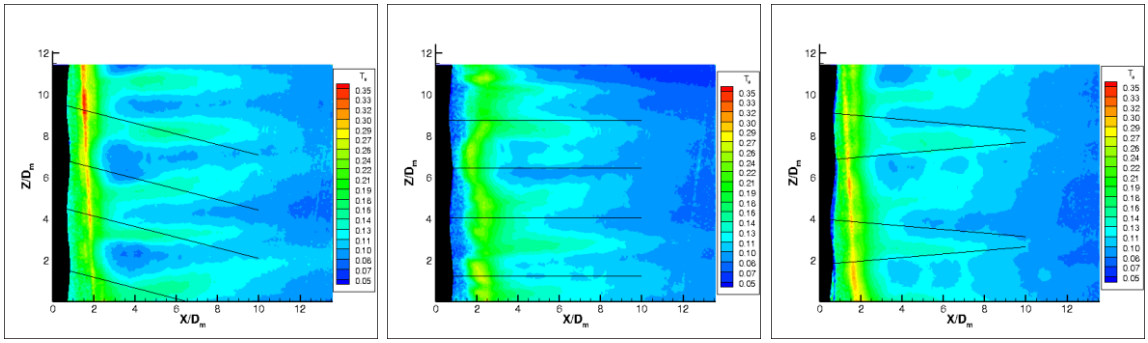

(a) Model C ($\alpha = -15^\circ$ $\beta = -15^\circ$) (b) Model A ($\alpha = 0^\circ$ $\beta = 0^\circ$) (c) Model B ($\alpha = 5^\circ$ $\beta = -5^\circ$)

Figure 10: Mean T_u Fields

Model B has a region of 20% T_u immediately following the whisker model. This is followed narrow band of much higher intensity between 27 to 33% T_u. The bands of 20% T_u angle away from the center point of the trough location. These bands of 20% T_u are significantly reduced by 10 D_m downstream of the whisker model. Regions of lower T_u can be found at the same Z/D_m as the peak and trough locations starting at 4 D_m downstream of the model.

Model C shows a region of 20% T_u immediately following the model. This is followed by a narrow region of higher T_u centered around 2 D_m downstream of the whisker model. Regions of lower T_u can be observed at the same Z/D_m positions that peak and trough point are located. The bands of 20% T_u extend at angles away from the trough center points. The T_u is reduced to 10% or less T_u by 10 D_m downstream of the model.

Figure 11 shows the T_u in the peak cross sectional plane. The half of the peak elliptical cross section is visible in black on the left edge of the figure.

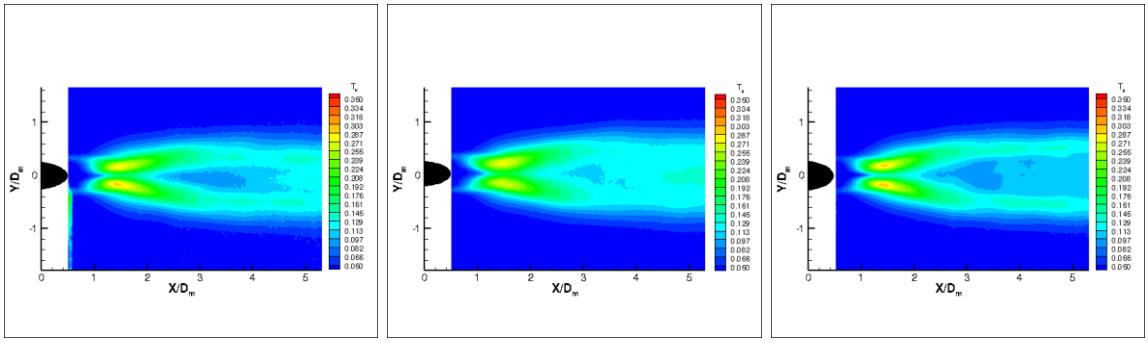

(a) Model C ($\alpha = -15^\circ$ $\beta = -15^\circ$) (b) Model A ($\alpha = 0^\circ$ $\beta = 0^\circ$) (c) Model B ($\alpha = 5^\circ$ $\beta = -5^\circ$)

Figure 11: Peak Mean T_u Field

Model A has a region of low T_u directly following the whisker model. This area of low intensity extends to 1.0 X/D_m downstream of the whisker model. Centered at 1.5 X/D_m extending from 1.2 to 2 X/D_m along the x-axis and above and below 0 Y/D_m are two pockets of high T_u reaching a maximum intensity of 30% T_u. The remainder of the wake is characterized by T_u in the 10 to 20% range. T_u above the free stream condition extends 1 D_m in both directions from the model centerline.

Model B has an area of low T_u following the model that extends to 1.0 X/D_m. There are two pockets of high T_u with magnitudes above 30%. These pockets begin at 1.2 X/D_m extend to 2 X/D_m. There is an area of lower T_u separating them along the model centerline. These pockets of high T_u are slightly angled away from the centerline in the downstream direction. The remainder of the wake is characterized by T_u in the 10 to 20% range. T_u greater than the free stream T_u is observed 1 D_m off the centerline in both directions. Model C has an area of low T_u following the model that extends to 1.2 X/D_m. There are two pockets of high T_u with magnitudes above 30%. These pockets begin at 1.3 X/D_m extend to 2.1 X/D_m. There is an area of lower T_u separating them along the model centerline. These pockets of high T_u are slightly angled

away from the centerline in the downstream direction. The remainder of the wake is characterized by T_u in the 10 to 20% range. T_u greater than the free stream T_u is observed 1 D_m off the centerline in both directions.

Figure 12 contains the T_u for the trough cross-sectional plane. The half of the trough elliptical cross section is visible in black on the left edge of the figure.

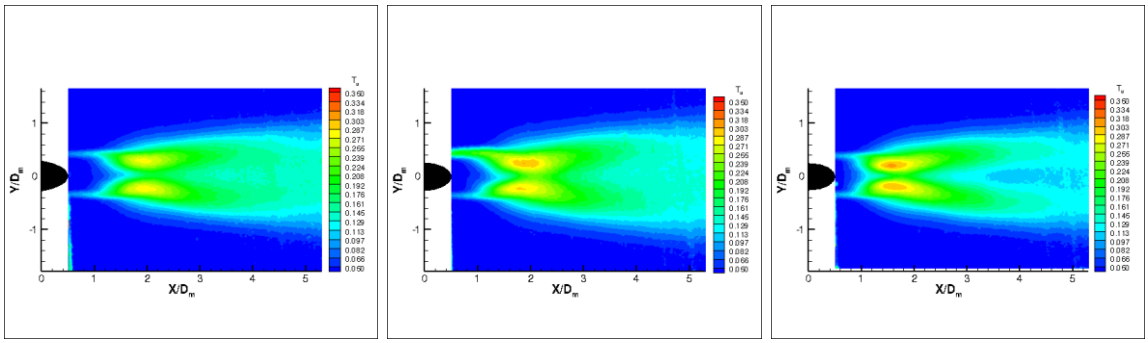

(a) Model C ($\alpha = -15^\circ$ $\beta = -15^\circ$) (b) Model A ($\alpha = 0^\circ$ $\beta = 0^\circ$) (c) Model B ($\alpha = 5^\circ$ $\beta = -5^\circ$)

Figure 12: Trough Mean T_u Fields

Model A has a low T_u region following the model that extends to 1.1 X/D_m downstream. There are two regions of high T_u on either side of the model centerline. These pockets are centered at 1.9 X/D_m and extend from 1.3 to 3 X/D_m downstream. The two pockets are oriented parallel to the model centerline and reach maximum magnitudes near 30% T_u. The remainder of the wake region is defined by T_u 15 to 20% range. The wake expands from the model to width of 2.8 D_m evenly distributed about the model centerline. Model B has a low T_u region following the model that extends to 0.8 X/D_m downstream. There are two regions of high T_u mirrored about the model centerline. These regions begin at 1.2 and extend to 2.7 X/D_m. The maximum magnitude of these pockets are located at 1.6 X/D_m and have magnitudes above 30% T_u. The remainder of the wake is characterized by T_u in the 12 to 20% range. The wake of T_u greater than the free stream T_u expands from the model to a maximum width of 2.4 D_m even distributed about the model centerline.

Model C has a low T_u region following the model that extends to 1.0 X/D_m downstream. There are two regions of high T_u mirrored about the model centerline. These regions begin at 1.2 and extend to 2.9 X/D_m. The maximum magnitude of these pockets are located at 1.8 X/D_m and have magnitudes maximizing at 30% T_u. The remainder of the wake is characterized by T_u in the 12 to 20% range. The wake of T_u greater than the free stream T_u expands from the model to a maximum width of 2.7 D_m even distributed about the model centerline.

V. Conclusion

Prior research of scaled up seal whisker models and computation models investigating the wake structure of the beaded seal whiskers focused on a very limited set of angles that find their origin with Hake et. al.[1, 6, 9, 10] While these angles of incidence fall within observed angles found in nature they are on the extreme edges of those found in nature.

The work conducted within this study looked at angles of α and β ranging from 0° to 15°. Attempting to cover the range observed within nature as well as investigate the direction of the angle as well as the magnitude of the angle of incidence. The three models used possessed the following angle of incidence; $\alpha = \beta = 0°$; $\alpha = \beta = 15°$, and $\alpha = 5° \beta = 5°$. From these models and the resulting flow studies it was observed that the angle of incidence can produce a significant effect on the flow structure. These effects can be summarized by; a re-organization of the pattern of velocity field, reduction in the distance required for velocity to recover, and enhanced mixing in the near and far wake with the inclusion of nonzero angle of incidence. These three functions of the angle of incidence are most clearly observed in the following cases.

Comparing u velocity field along the vertical centerline plane in model A to the model B and observing a complete switch with peaks recovering fastest in the model A case to slowest in the model B. The overall reduction of distance required for fully recovered u velocity field most notably observed in vertical centerline plane as well as the trough cross-sectional planes when comparing the model C to the model A.

Finally the enhanced mixing could be observed in the removal of the strongly ordered u field observed in both models A and B in the vertical centerline plane that is not observable in the model C. The reduction

in the low Tu zone following the model observed in model C at the trough cross-section also adds to the final finding of enhanced mixing.

From these results it can be understood that an intelligently designed whisker like geometry can provide enhanced performance advantages over whisker geometry that possess a constant angle of incidence. Namely this study found that an alternation of direction for α and β can provide substantial performance gains.

Acknowledgments

The authors would like to acknowledge the efforts of fellow graduate students Joseph Bunjevac and Justin Flarety for their assistance in setting up the water channel and PIV system as well as their help in conducting these experiments. In addition authors would like to thank Dr. Borkar and Prashanth Yennam for their expertise in 3D printing and help in building the whisker models utilized within this study.

References

[1]Hanke, W.,Witte, M., Miersch, L., Brede, M. Oeffner, J. Michael, M. Hanke, F. Leder, " Harbor Seal Vibrissae Morphology Suppresses Vortex-Induced Vibrations" , *The Journal of Experimental Biology*,Vol. 213, pp. 2665-2672, 2010.

[2]Ginter, C., DeWitt, T., Fish, F., Marshall, C., " Fused Traditional and Geometric Morphometrics Demonstrate Pinniped Whisker Diversity," PLoS ONE Vol. 7, No. 4, Apr. 2012.

[3]C. Ginter, F. Fish, C. Marshall, " Morphological analysis of the bumpy profile of phocid vibrissae" , *Marine Mammal Science*, volume 26, pp. 733-743, 2010.

[4]Murphy, C., Eberhardt, W., Calhoun, B., Mann, K., Mann, D., " Effect of Angle on Flow-Induced Vibrations of Pinniped Vibrissae," PLoS ONE, Vol. 8, No. 7, Jul 2013.

[5]C. Murphy, Structure and Function of Pinniped Vibrissae, PhD Dissertation, University of South Florida, 2013.

[6]Hans, H., Miao, J., Triantafyllou, M., Weymouth, G., " Whisker-like Geometries and Their Force Reduction Properties," OCEANS MTS/IEEE Conference, Bergen Norway, 2013.

[7]Y.F. Lin, H.L. Bai, Md. Mahbub Alam, W.G. Zhang, K. Lam, " Effects of large spanwise wavelength on the wake of sinusoidal wavy cylinder" , *Journal of Fluids and Structures*, volume 61, pp. 392-409 2016.

[8]G. Dehnhardt, B. Mauck, W. Hanke, H. Bleckmann, Hydrodynamic trail following in harbor seals(Phoca vitulina). *Science* volume 293, pp. 102-104 2001.

[9]Beem, H., " Passive Wake Detection Using Seal Whisker-Inspired Sensing," PhD Dissertation, Joint Program in Oceanography and Applied Ocean Science and Engineering, MIT and WHOI, Cambridge, Mass., 2015.

[10]Shyam, V., Ameri, A., Poinsatte, P., Thurman, D., Wroblewski, A., Snyder, C., " Application of Pinniped Vibrissae to Aeropropulsion," Proceedings of ASME Turbo Expo, Montreal Canada, Jun 2015.

[11]DeArmon, E., Stone, M., Rogenski, E., Thurman, D., Poinsatte, P., Shyam V., " Characterization and Analysis of Phoca Vitulina, Zalophus Californianus and Mirounga Angustirostris Vibrissae" , NASA TM (in publication), 2016.

[12]Rinehart, A., Zhang, W., " Characterization of Seal Whisker Morphology and Effects on Wake Flow Structure," AIAA Region III Student Conference, Champaign-Urbana, IL, 2016.

[13]Wagner, J., ?Karmansche Wirbelstrabe grobe Reynoldszahl," Wikimedia, Oct. 2014., https://commons.wikimedia.org/wiki/File:Karmansche_Wirbelstr_groC39Fe_Re.JPG, cited 2 Mar. 2016.